Chemical Engineering Journal 244 (2014) 569–575

Contents lists available at ScienceDirect

Chemical Engineering Journal

journal homepage: www.elsevier.com/locate/cej

Highly efficient removal of Cr(VI) from water with nanoparticulated zerovalent iron: Understanding the Fe(III)–Cr(III) passive outer layer structure

V. Nahuel Montesinos [a,b,c], Natalia Quici [a,b], E. Beatriz Halac [d], Ana G. Leyva [c,e], Graciela Custo [a], Silvina Bengio [f], Guillermo Zampieri [b,g], Marta I. Litter [a,b,d,h,*]

[a] Gerencia Química, Comisión Nacional de Energía Atómica, Av. Gral. Paz 1499, 1650 San Martín, Prov. de Buenos Aires, Argentina
[b] Consejo Nacional de Investigaciones Científicas y Técnicas, Av. Rivadavia 1917, 1033 Ciudad Autónoma de Buenos Aires, Argentina
[c] Departamento de Química Inorgánica, Analítica y Química Física, FCEN, Universidad de Buenos Aires, Ciudad Universitaria Pabellón II, 1428 Ciudad Autónoma de Buenos Aires, Argentina
[d] Gerencia de Investigación y Aplicaciones, Comisión Nacional de Energía Atómica, Av. Gral. Paz 1499, 1650 San Martín, Prov. de Buenos Aires, Argentina
[e] Escuela de Ciencia y Tecnología, Universidad de Gral. San Martín, Campus Miguelete, Martín de Irigoyen 3100, 1650 San Martín, Prov. de Buenos Aires, Argentina
[f] Instituto Balseiro, Universidad Nacional de Cuyo, Av. Bustillo 9500, 8400 Bariloche, Prov. de Río Negro, Argentina
[g] Centro Atómico Bariloche, Comisión Nacional de Energía Atómica, Av. Bustillo 9500, 8400 Bariloche, Prov. de Río Negro, Argentina
[h] Instituto de Investigación e Ingeniería Ambiental, Universidad Nacional de Gral. San Martín, Peatonal Belgrano 3563, 1° piso, 1650 San Martín, Prov. de Buenos Aires, Argentina

HIGHLIGHTS

- An outstanding Cr(VI) removal was achieved with these nZVI in only 30 min.
- The passive outer layer formed after treatment prevents further Cr(VI) removal.
- Cr(III) is the only chromium species at the external layer after reaction.
- A structure of hydroxychromites → magnetite → Fe^0 developed towards the core of the nZVI.

ARTICLE INFO

Article history:
Received 3 September 2013
Received in revised form 26 January 2014
Accepted 29 January 2014
Available online 6 February 2014

Keywords:
Hexavalent chromium
Nanoscale zerovalent iron
XPS analysis
Raman spectroscopy

ABSTRACT

Nanoscale zerovalent iron (nZVI) particles were successfully employed for Cr(VI) removal from aqueous solutions at pH 3. It was found that the capacity of the system increases with increasing nZVI dosage. Starting at 300 μM, a complete Cr(VI) conversion was achieved in 30 min with a Fe:Cr(VI) molar ratio (*MR*) of 3, and 45% conversion with *MR* = 1 over the same period of time. The material exhibited an enhanced reactivity in comparison with other previously tested similar materials.

The proposed mechanism involves an initial reduction of Cr(VI) to Cr(III) by reaction with Fe^0 or Fe(II) on the particle surface or in solution (secondary pathway), followed by an arrest on Cr(VI) removal attributed to the passivation of the surface of the nanoparticles. Passivation was confirmed by Raman and X-ray photoelectron spectroscopies (XPS). Furthermore, XPS analysis demonstrated that Cr(III) is the only Cr species present in the external layer of the nanoparticles after the reaction. Raman analysis and XPS measurements performed after mild sputtering showed that nZVI exposed to Cr(VI) presented a structure, from outside to inside, of hydroxychromites → magnetite → Fe^0.

1. Introduction

Hexavalent chromium is the Cr species that presents the highest environmental threat in aqueous systems, due to its toxicity to biological organisms, high solubility and mobility. The toxicological effects of Cr(VI) originate on its oxidative nature in water, as well as on the formation of free radicals during the reduction of Cr(VI) to Cr(III) occurring inside the cell [1]. Consequently, the World Health Organization [2] recommends a 0.05 mg L^{-1} maximum contaminant level of Cr(VI) in drinking water, while total chromium should be discharged below 2 mg L^{-1} according to US EPA regulations [3].

* Corresponding author at: Gerencia Química, Comisión Nacional de Energía Atómica, Av. Gral. Paz 1499, 1650 San Martín, Prov. de Buenos Aires, Argentina. Tel.: +54 011 6772 7942.
E-mail addresses: litter@cnea.gov.ar, marta.litter@gmail.com (M.I. Litter).

http://dx.doi.org/10.1016/j.cej.2014.01.093
1385-8947/

In the last two decades, it has been demonstrated that zerovalent iron (ZVI) materials are a good alternative for the removal of a wide range of pollutants including metals and metalloids in water, showing a high efficiency and low economic and environmental costs [4–9]. More recently, the use of ZVI nanoparticles (nZVI) proved to be a promising and more efficient version of this technology [10–17]. In addition to showing an enhanced reactivity, their larger surface area and higher penetrability in soil make these particles also a very powerful tool for on-site treatment. In particular, Cr(VI) sequestration with ZVI [18–22] and nZVI [23–29] has been extensively studied. The general process can be described as the reduction of Cr(VI) to Cr(III) coupled with the oxidation of Fe^0 to Fe(II) and Fe(III), and the subsequent precipitation of sparingly soluble iron hydroxychromites [4].

Due to its reductive nature and to the fact that the corrosion of the material is thermodynamically favoured in the presence of oxygen, ZVI particles unavoidably develop a thin film of oxides on the surface, being extensively accepted that this external film has a fundamental role on Cr(VI) sequestration. The protective layer of iron oxides continuously grows at the Fe^0/oxide layer interface while being simultaneously destroyed by dissolution or restructuring at the oxide layer/H_2O interface. A porous structure, which can be considered multi-layered, with increasing density from the external oxide layer to the metallic core, is created [30]. The passive film is generally described by a two-layer model constituted by magnetite (Fe_3O_4) and maghemite (γ-Fe_2O_3) [31,32]. The variable arrangement of the oxides forming the shell has been described by several models, e.g.: (a) an inner layer of Fe_3O_4 and a γ-Fe_2O_3 outer layer at the oxide-solution interface, (b) less discrete layers constituted by amorphous oxides, or (c) a layer of mixed oxides with a Fe(II) concentration gradient decreasing from Fe_3O_4 to γ-Fe_2O_3 towards the surface [31,32]. The electron transfer from the Fe^0 core to the contaminants depends strongly on the composition of this layer, which can act as a semiconductor or coordinating surface [32] and affects the mass transport [30]. Fe^0 can be regarded as a long-term source of highly reactive hydroxides or oxides [33].

In this work, Cr(VI) removal in aqueous solution was analyzed by using very reactive commercial nZVI particles at different Fe:Cr(VI) molar ratios (*MR*). The effect of the *MR* used in the Cr(VI) removal was evaluated and a possible mechanism was postulated.

2. Materials and methods

2.1. Chemicals

Cr(VI) solutions were prepared using $K_2Cr_2O_7$ provided by Mallinkrodt. nZVI (NANOFER 25, hereafter N25) was provided by NANO IRON, s.r.o. (Czech Republic) as a suspension in water and kept at low temperature (~4 °C) until used. *o*-phenantroline (Mallinckrodt), H_2SO_4 (Biopack), ascorbic acid (Carlo Erba), 1,5-diphenylcarbazide (UCB), phosphoric acid (Biopack) were of analytical reagent grade and used without further purification. In all experiments, Milli-Q water was used (resistivity = 18 MΩ cm).

2.2. Experimental setup

Batch experiments were carried out in a 400 mL cylindrical jacketted Pyrex glass reactor. Temperature was controlled by recirculating water through the jacket using a Polyscience 9106 Circulator, and the content was stirred by a vertical paddle agitator (Decalab). The experimental setup is shown in Fig. S1 of the Supplementary data (SD).

Preliminary experiments were performed at pH 3, 5 and 7 and, from them, pH 3 was chosen as the working pH for most experiments. All experiments were carried out with 200 mL of 300 μM Cr(VI) solution, previously adjusted at pH 3 with 0.2 M H_2SO_4 and open to the atmosphere. Cr(VI) solutions were stirred for 15 min to achieve oxygen saturation before each experiment (7.2–7.6 mg L^{-1}), and no change in [O_2] took place during Cr(VI) removal with N25. Finally, nZVI particles were added to the system in the 150–900 μM range (expressed as total Fe), corresponding to a Fe:Cr(VI) *MR* range of 0.5–3. A few additional experiments were carried out at pH 5, keeping all other conditions equal, with nZVI in the 300–3000 μM range.

2.3. Analytical methods

In all experiments, 4 mL samples were periodically withdrawn and separated in four 1 mL aliquots, which were centrifuged in Eppendorf tubes during 2 min using an Eppendorf MiniSpin® centrifuge at 13,000 rpm. The supernatant of each sample was used separately for Cr(VI), Fe(II), Fe_{total} and Cr_{total} analysis. [Cr(VI)] was measured spectrophotometrically using the diphenylcarbazide method at 540 nm [34]. [Fe(II)] and [Fe_{total}] were measured spectrophotometrically using the *o*-phenanthroline method at 508 nm [35]. UV–vis absorption measurements were performed employing a UV–visT80+ spectrophotometer (PG instrument Ltd.). [Cr_{total}] was measured employing Total Reflection X-ray Fluorescence (TXRF) [36] using a solution of [Co(II)] = 10 μM as internal standard. A total reflection system comprising an X-ray spectrometer, an X-ray tube excitation system, a total reflection module and spectrum acquisition and quantitation software was used. The X-ray spectrometer consisted of an 80 mm Si(Li) detector with 166 eV of full width half maximum (FWHM) for 5.9 keV, a 0.008 mm thick Be window, an Ortec 672 fast spectroscopy amplifier and an analog-to-digital converter (ADC) Nucleus PCA2. Excitation conditions were 50 kV and 30 mA in all cases and the spectrum acquisition time was 300 s in every case. Initial and final pH determinations were carried out using a pH-meter (Meterlab PH M210), and dissolved O_2 was measured with an oxygen sensor (Hach Sens Ion 156 Multiparameter Meter) equipped with a Hach DO meter electrode. As shown in Ref. [29] temperature is a determinant parameter in Cr(VI) removal by nZVI, therefore all experiments were performed at 24 ± 1 °C at least by duplicate, and the results averaged. The experimental error was calculated as the standard deviation of replicate experiments and was never higher than 10%.

2.4. nZVI characterization

X-ray diffraction (XRD), Raman spectroscopy and XPS analysis were carried out to characterize nZVI particles before and after exposure to Cr(VI). After the treatment, the solid particles were filtered using 0.22 μm cellulose acetate membranes (Osmoionics), washed three times with 2 mL Milli-Q water and preserved under vacuum for 24 h before the analysis. XRD patterns were obtained with a Philips PW-3710 X-ray diffractometer, using Cu Kα radiation. Data for Raman spectroscopic measurements were acquired in a LabRAM HR Raman system (Horiba JobinYvon), equipped with a confocal microscope, two monochromator gratings and a charge coupled device detector (CCD). An 1800 g/mm grating and 100 μm hole results in a 2 cm^{-1} spectral resolution. The 514.5 nm line of an Ar^+ laser was used as the excitation source. Measurements were carried out in a backscattering geometry, with an objective magnification of 50×. Acquisition time was 180 s and 4 accumulations. XPS spectra were taken with a hemispherical electrostatic energy analyzer (r = 10 cm) using Al Kα radiation ($h\nu$ = 1486.6 eV). Mild sputtering experiments were performed with an Ar beam of 2 keV ion energy and a current density of around 10 μA cm^{-2}; in these conditions, a sputtering rate of a few Å min^{-1} is expected.

Scanning electron microscopy (SEM) analysis was performed with a Q200 FEI Company equipment only for N25 samples. In this case, suspended nanoparticles were seeded in a copper–aluminium support and dried under vacuum 24 h before the analysis. The supported sample was coated with a thin gold film to improve its conductivity and, therefore, the resolution of SEM images.

3. Results and discussion

3.1. N25 characterization

The nanoparticles present a core–shell like structure with a Fe^0-rich core surrounded by a magnetite-rich shell. The most important characteristics of the N25 particles, are presented in Table S1 (SD). Fig. S2(a) (SD) shows the X-ray diffraction pattern of the commercial nanoparticles, where two distinct phases can be distinguished: one corresponding to α-Fe, and the second one assigned either to magnetite and/or to maghemite. Those two phases cannot be differentiated by the technique under our experimental conditions. However, this ambiguity was resolved by Raman spectroscopy, displayed in Fig. S2(b), which indicates that the only iron oxide phase present in the initial nZVI sample is magnetite. The mean crystallite size was estimated from the FWHM of the α-Fe peak located at 45°, using the Scherrer equation. The obtained value was approximately 70 nm, in close agreement with the results provided by the manufacturer. The SEM image of fresh N25 particles is shown in Fig. S3 (SD). It can be observed that the freshly seeded material is disposed as irregular agglomerates with a fine structure composed of spherical nanoparticles with an estimated diameter of 65 nm.

The characterization analysis confirmed all data provided by the supplier.

3.2. Experiments of Cr(VI) removal

Results of the experiments aimed at evaluating the performance of N25 particles on Cr(VI) removal at pH 3 are displayed in Fig. 1. This working pH was selected after a series of preliminary experiments at pH 3, 5 and 7, because this condition showed the highest reactivity and allowed a good inspection of the temporal concentration profiles. At higher pH values, removal efficiency was much lower.

As it can be observed in Fig. 1(a), removal of dissolved Cr(VI) increased with the initial nZVI mass, with complete removal with [nZVI] = 900 μM (*MR* 3) after 30 min. A very rapid initial Cr(VI) conversion during the first 10 min was followed by a plateau in all cases. Therefore, the maximum Cr(VI) removal was reached in only 10 min. As the best (complete) conversion was found for *MR* 3 at 30 min, the percentage of Cr(VI) removed after that time for all *MR* was plotted against the amount of nZVI. Fig. 1(b) indicates a linear behaviour, with the exception of *MR* 3, where the nZVI particles seem to still preserve Cr(VI) removal power.

The performance obtained in this work is the highest registered for Cr(VI) removal with nZVI to our knowledge, in comparison with previous works. Table 1 lists the Cr(VI) removal efficiency of different nanoparticulated materials in terms of mg of Cr(VI) removed per gram of nZVI, taken from the literature [24,25,27].

In order to achieve a better understanding of the system, concentrations of Fe(II), Fe(III) and Cr_{total} were measured during the time span of the reaction. *MR* 1 was chosen to allow a proper inspection of the experimental data; results are displayed in Fig. 2.

Fig. 2 shows that around 50% of Cr(VI) is removed after 120 min, leaving Cr(III) in solution and 94% of total chromium still dissolved, indicating that direct Cr(VI) adsorption does not take place under our experimental conditions or at least it could not be perceived due to fast reduction on the surface. Additionally, it can be observed that Cr(VI) removal is coupled with a partial dissolution of the nanoparticles introducing iron in the aqueous phase; both processes, removal and dissolution stop simultaneously after 10 min.

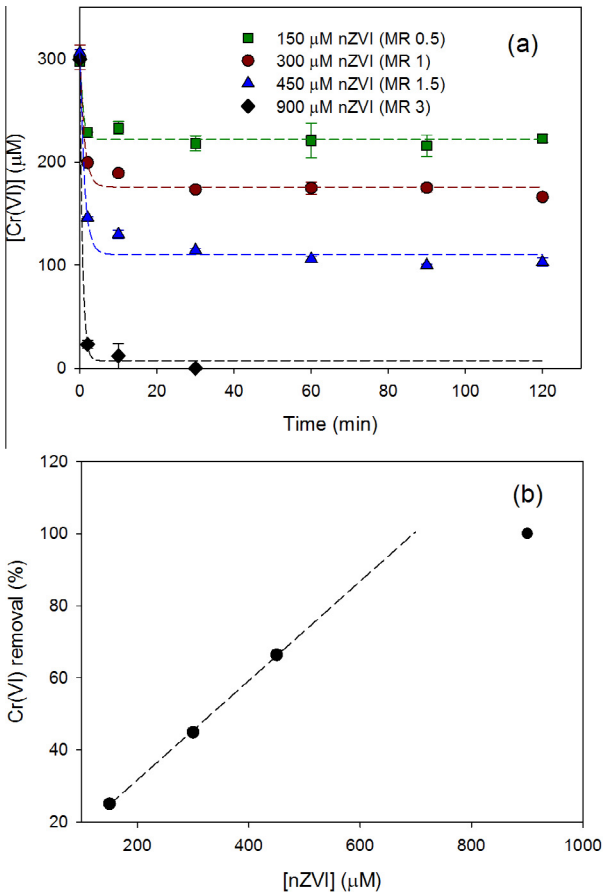

Fig. 1. (a) [Cr(VI)] vs. time for removal experiments with different *MR* and (b) percentage of Cr(VI) removal after 30 min of treatment vs. [nZVI]. Conditions: [Cr(VI)] = 300 μM, pH 3, $T = 24 \pm 1$ °C. Dashed curves are only for better visualization of points and do not correspond to a fitting model.

Table 1
Mass of Cr(VI) removed per gram of nZVI for different nZVI materials.

mg Cr(VI)/g nZVI	pH	Reference
10.06	6.36	Ai et al. [25]
50–180	4–8	Li et al. [24]
34.1	6	Kim et al. [28]
62.4	6	Wang et al. [26]
20.16	5	Alidokht et al. [27]
180	4.82	Fang et al. [37]
100	3	Lv et al. [38]
47.2 ± 0.1	5	This work
411 ± 24	3	This work

The main proposed pathway for Cr(VI) removal by ZVI materials [22] comprises the heterogeneous Cr(VI) reduction involving direct electron transfer from Fe^0 ($E^0_{Fe^{2+}/Fe^0} = -0.44$ V) to Cr(VI) ($E^0_{HCrO_4^-/Cr^{3+}} = 1.36$ V):

$$2HCrO_4^- + 14H^+ + 3Fe^0(s) \rightarrow 2Cr^{3+} + 8H_2O + 3Fe^{2+} \quad (1)$$

As postulated in Ref. [39], Cr(VI) can be reduced by Fe(II) at the surface (indicated as ≡Fe(II), Eq. (2)), as Fe(II) in the solid is a more reducing species than Fe(II) in solution (indicated as Fe^{2+}) [40]. Further regeneration of ≡Fe(II) can occur after the surface reaction between Fe^0 with ≡Fe(III) (Eq. (3)):

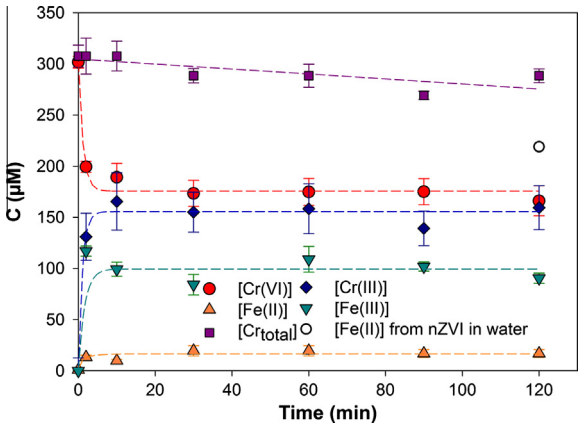

Fig. 2. Time profiles of [Cr(VI)], [Cr(III)], [Fe(II)], [Fe(III)] and [Cr_{total}] for Cr(VI) treatment with nZVI. Conditions: [Cr(VI)] = 300 μM, [nZVI] = 300 μM (*MR* 1), pH 3, T = 24 ± 1 °C. [Fe(II)] from [nZVI] = 300 μM in water after 120 min at pH 3 and T = 24 ± 1 °C is also plotted as an open circle. Dashed curves are only for better visualization of points and do not correspond to a fitting model.

$$HCrO_4^- + 7H^+ + 3 \equiv Fe(II) \rightarrow Cr^{3+} + 3 \equiv Fe(III) + 4H_2O \quad (2)$$

$$Fe^0 + 2 \equiv Fe(III) \rightarrow 3 \equiv Fe(II) \quad (3)$$

On the other hand, a minor pathway that cannot be fully ruled out at pH 3 [38] involves the homogenous Cr(VI) reduction by dissolved Fe^{2+} ions (Eq. (4)), having the same stoichiometry than Eq. (2) but with less reducing power [40].

$$HCrO_4^- + 7H^+ + 3Fe^{2+} \rightarrow Cr^{3+} + 3Fe(III) + 4H_2O \quad (4)$$

Only 11% of the initial Cr(VI) could be removed through this minor pathway (Eq. (4)), as it can be calculated by mass balance and using the concentrations of iron species from Fig. 2. Fang et al. [37] measured the extent of this pathway by capturing dissolved Fe^{2+}, and found a reduction in Cr(VI) removal efficiency of 7.4%, in good agreement with the 11% estimated in this work. Thus, the overall reaction for Cr(VI) reduction by nZVI is represented by Eq. (5):

$$HCrO_4^- + 7H^+ + Fe^0(s) \rightarrow Cr^{3+} + 4H_2O + Fe^{3+} \quad (\text{or} \equiv Fe(III)) \quad (5)$$

Consistently with Eq. (5), in all experiments, a slight increase in pH (≈ΔpH = 0.4) was observed.

Even though it is not possible to determine the exact extent of Cr(VI) reduction by Fe^{2+} compared with the reduction at the surface of the nanoparticles (Eqs. (1) and (4)), the fact that iron dissolution and Cr(VI) removal stopped simultaneously at 30 min (Fig. 2) evidences a connection between these two processes. The arrest in Cr(VI) removal together with the interrupted iron dissolution would indicate the poisoning of the nZVI surface. This is in accordance with the precipitation of Cr(III) at the surface as amorphous $Cr(OH)_3$ [18,41] or Fe(III)–Cr(III) hydr(oxydes) that has been previously associated with the passivation of the surface of iron nanoparticles [24]. The formation of the solid compounds is represented by Eqs. (6)–(8):

$$Cr^{3+} + 3H_2O \rightarrow Cr(OH)_3(s) + 3H^+ \quad (6)$$

$$xCr^{3+} + (1-x)Fe^{3+} + 3H_2O \rightarrow (Cr_xFe_{1-x})(OH)_3(s) + 3H^+ \quad (7)$$

$$xCr^{3+} + (1-x)Fe^{3+} + 2H_2O \rightarrow Cr_xFe_{1-x}OOH(s) + 3H^+ \quad (8)$$

The surface passivation hypothesis was supported by the fact that the amount of Fe(II) found in solution after 120 min of stirring nZVI (300 μM) in water in the absence of Cr(VI) (Fig. 2) [Fe^{2+}] was higher than in the same experiment with Cr(VI) (219 against 16 μM, respectively).

It is worth mentioning that direct corrosion of the nZVI particles by O_2 is not likely to be extensively developed under the present experimental conditions since their oxidation by Cr(VI) is thermodynamically and kinetically favoured ($E^0_{HCrO_4^-/Cr^{3+}}$ is 1.36 V, i.e., more positive than that of O_2/H_2O (1.23 V)). In agreement, as said in the experimental section, preliminary experiments showed that no changes in the concentration of oxygen took place during Cr(VI) removal with N25.

As a final refinement of the process, the product of the reaction, Cr(III), could be removed in a subsequent step by alkalinization. As known, Cr(III) toxicity and mobility is lower than that of Cr(VI) and, hence, the removal process is able to reduce the toxicity of the initial solution. Fe(II) and Fe(III), which are non-toxic, remain in solution as 0.94 and 5.04 mg L^{-1}, respectively (Fig. 2) and would be precipitated also by the alkalinization step.

3.3. XRD and Raman analysis of the solids

Fig. 3(a) compares the XRD pattern of the initial N25 particles sample with that of the solid obtained after 120 min of contact

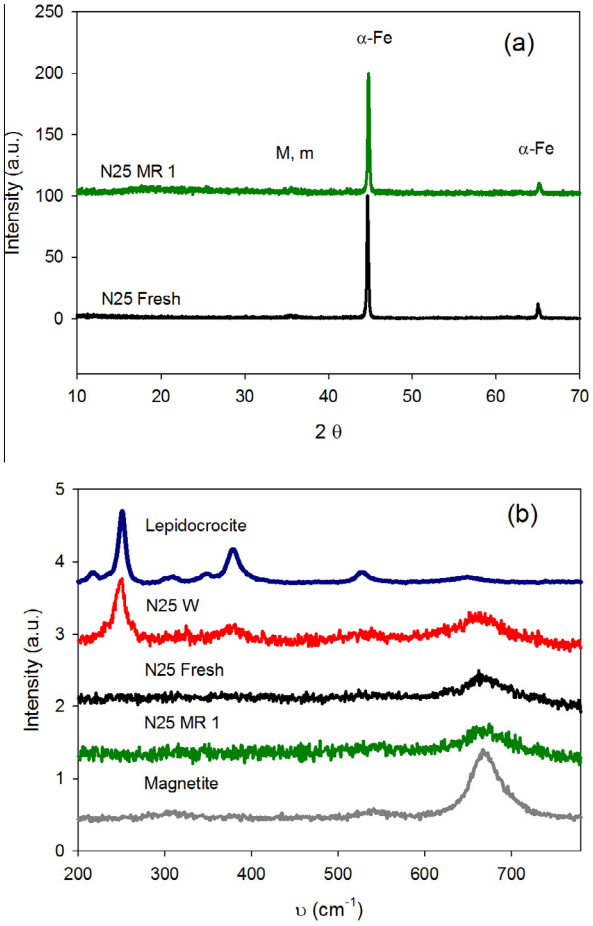

Fig. 3. (a) X-ray diffraction patterns of nZVI particles before (N25 Fresh) and after 120 min of Cr(VI) treatment with *MR* 1 (N25 MR 1). Magnetite (M), maghemite (m) and α-Fe reference peaks are indicated. (b) Raman spectra of fresh N25 particles (N25 Fresh), nZVI after 120 min in contact with Cr(VI) at *MR* 1 (N25 MR 1), and after 120 min in water in the absence of Cr(VI) (N25 W). Conditions: pH 3, T = 24 ± 1 °C. Raman spectra of pure lepidocrocite and magnetite samples are also displayed.

with Cr(VI) (*MR* 1). It can be seen that, after Cr(VI) treatment, no evidence of new iron phases is observed. Fig. 3(b) shows the Raman spectra of fresh N25 particles, the solid after 120 min of Cr(VI) treatment at *MR* 1 (N25 MR 1), and the solid obtained after 120 min when N25 was in contact with water in the absence of Cr(VI) (N25 W). Spectra of pure lepidocrocite and magnetite samples are also shown. When nZVI was in contact with Cr(VI), the only iron oxide phase present after 120 min was magnetite, as in the original material. However, in the absence of Cr(VI), lepidocrocite was detected in addition to the magnetite phase. Lepidocrocite is an Fe(III) oxyhydroxide commonly formed as an electrochemical corrosion product of iron in acid media in excess of dissolved O_2 (>3 mg L^{-1}) [42], conditions existing actually in our system, as indicated in the experimental section. The fact that lepidocrocite is not formed in the presence of Cr(VI) strongly suggests that Cr(VI) reduction at the surface of nZVI particles prevents further changes in the outer layer. In this way, neither Cr(VI) reduction nor corrosion can further occur.

3.4. XPS analysis of nZVI before and after Cr(VI) removal experiments

Fig. 4 shows the XPS spectra taken for samples of N25 before treatment (N25 Fresh) and after treatment of a Cr(VI) solution with *MR* 1. Both samples present the spin–orbit split Fe 2p peaks at around 711 and 724 eV with signals composed of photoelectrons from Fe^0, Fe(II) and Fe(III) (Fig. 4(a)) and a broad O 1s peak at 531 eV with contributions of $\equiv O^-$, $\equiv OH$ and $\equiv OH_2$ components (Fig. 4(b)). The peak fitting methodology description is provided in the SD, especially indicated for the case of the Fe 2p spectra in Fig. S4. After 120 min treatment with 300 μM Cr(VI), two new peaks appeared at 577 and 586 eV, corresponding to the Cr $2p_{3/2}$–$2p_{1/2}$ photoelectrons (Fig. 4(c)). The binding energies (BE) and the spin–orbit splitting of the Cr 2p peaks are in good agreement with those reported for Cr_2O_3 or $Cr(OH)_3$ [43]. This indicates that Cr(III) is the only species present at the surface, in agreement with the fact that Cr(VI) adsorption does not take place or, if it takes place, Cr(VI) is instantaneously reduced on the surface. A detailed analysis shows that the maximum of the Fe $2p_{3/2}$ peak shifts from 710.8 eV in the fresh material to 711.5 eV after the Cr(VI) treatment (Fig. 4(a)), consistent with oxide and hydroxide environments, respectively. The analysis of the O 1s peaks (Fig. 4(b)) supports this concept by showing an increase in the proportion of $\equiv OH$ and $\equiv OH_2$ over $\equiv O^-$ components after the treatment. Being the mean free path for iron equivalent to 6 atomic layers, in the case of a monolayer of Cr(III) adsorbed on the surface of the nZVI particles, an approximate ratio of Cr:Fe intensities = 1:5 would have been expected as the mean free path and the photoemission cross section of Fe 2p and Cr 2p are similar [43]. However, in the *MR* 1 sample, the analysis of the Cr:Fe intensity ratio indicates a 1:1 value which denotes that Cr(III) is incorporated into the solid structure.

Formation of alloy-like passivating Cr–Fe hydroxides on the surface of nZVI has been reported previously [6,23,24]. Manning et al. [23] studied the solid product obtained after Cr(VI) treatment with nZVI by EXAFS, XANES and XPS, finding that only Cr(III) is retained in the surface as a poorly ordered $Cr(OH)_3$ and/or a mixed phase of $Cr_xFe_{1-x}(OH)_3$. Li et al. [24] analyzed the chromium deposition on the nZVI surface using high-resolution X-ray photoelectron spectroscopy (HR-XPS), finding the stoichiometry of the chromites to be approximately Cr/Fe 2:1, i.e. $(Cr_{0.67}–Fe_{0.33})(OH)_3$ or $Cr_{0.67}Fe_{0.33}OOH$. According to the authors, after reaching the oxide surface of the nanoparticles, Cr(VI) would be initially reduced to $Cr(OH)_3$ and then incorporated to the FeOOH structure in the form of chromites.

In order to analyze the nZVI particles composition as a function of depth from the surface before and after Cr(VI) treatment, mild sputtering experiments were performed; XPS spectra of N25 Fresh and *MR* 1 samples were taken over time. Fig. 5 shows the relative concentration of Fe^0, Fe(II), Fe(III) and Cr(III) in the exposed surface over sputtering time for the *MR* 1 sample. The relative concentration of the iron phases was calculated as $[Fe\ 2p]_i/[Fe\ 2p]_T$, where $[Fe\ 2p]_i$ is the total area of the peak of the *i*th iron component and $[Fe\ 2p]_T$ the total Fe 2p signal for each sample. For Cr(III), the relative concentration was calculated as $[Cr\ 2p]_t/[Cr\ 2p]_0$, where $[Cr\ 2p]_t$ is the area of the Cr 2p peak at time "*t*" and $[Cr\ 2p]_0$ the area of the Cr 2p peak at time "0". A clear increase in the Fe^0 signal is observed, and it proves that the sputtering is removing the external iron oxide shell from the nanoparticles. As said before [27,28], several models have been used to describe the iron oxide film from a two-layer discrete model to a gradient of mixed oxides. In our case, a more complete description of the layer can be obtained after the XPS results because an increase in the Fe(II):Fe(III) ratio

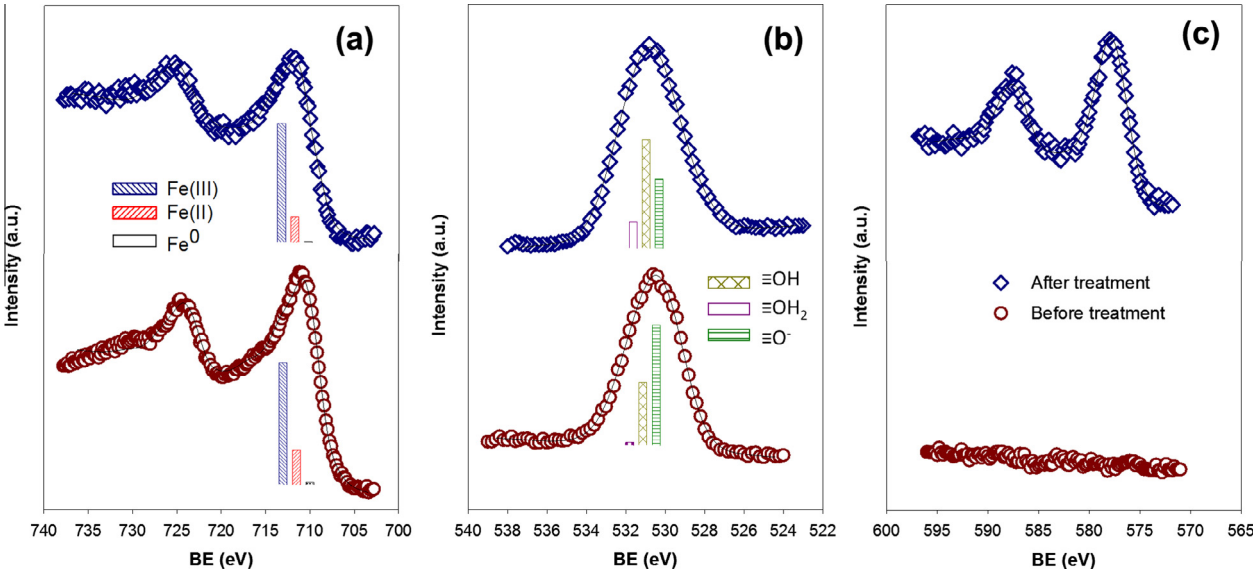

Fig. 4. XPS spectra of fresh N25 particles (lower curve) and after 120 min of Cr(VI) treatment with *MR* 1 (upper curve): (a) Fe 2p, (b) O 1s and (c) Cr 2p. Conditions: [Cr(VI)] = 300 μM, pH 3, $T = 24 \pm 1$ °C. The intensity scale (a.u.) is the same for Fe 2p, O 1s and Cr 2p peaks.

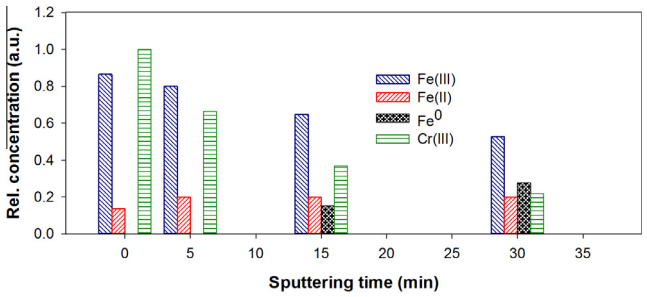

Fig. 5. Time evolution of relative concentrations of Fe^0, Fe(II), Fe(III) and Cr(III) in N25 MR 1.

indicates that the structure of the oxide film is a Fe(II)–Fe(III) iron oxide with a continuous Fe(II) gradient towards the interior of the nanoparticles, consistent with the detection of a magnetite phase by Raman spectroscopy.

On the other hand, a clear decrease in Cr(III) concentration is observed as long as the oxide film is removed by sputtering, revealing that Cr is trapped only in the surface of the nZVI, leaving a still reactive Fe^0 enriched core that cannot be exploited for Cr(VI) removal, due to the formation of a Cr(III)–Fe(III) passive film.

As revealed by Fig. 6(a) and (b), as long as the sputtering removes layers from the nZVI after treatment, a clear decrease in the BE of Cr(III) and Fe(III) is observed. This behaviour corresponds to the transition from a more hydroxy/oxyhydroxy environment to a pure oxide phase and is consistent with the composition of oxygenated species displayed in Fig. 6(c). The intensity of oxygen forming ≡OH and $\equiv OH_2$ increases after the treatment and decreases after 30 min of sputtering, where the $\equiv O^-$ component is dominant. This is not the case of N25 Fresh, where, as shown in Fig. 6, the BE hardly changes with sputtering time and the environment is constituted only by $\equiv O^-$.

As indicated before, Cao and Zhang [21] calculated the stoichiometry of Cr(III) incorporated to the FeOOH structure as $(Cr_{0.67}–Fe_{0.33})(OH)_3$ or $Cr_{0.67}Fe_{0.33}OOH$. However, this stoichiometry relay on the assumption of a constant Cr:Fe ratio for the

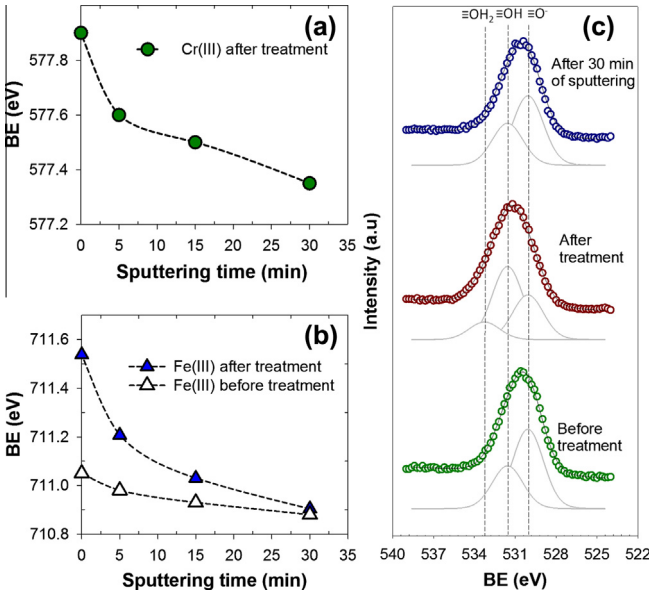

Fig. 6. BE shifts over sputtering time for (a) Cr(III), (b) Fe(III) peaks, centred around 577.5 and 710.5 eV, before and after treatment of a Cr(VI) solution in a *MR* 1 and (c) O 1s XPS spectra before and after treatment and after 30 min of sputtering. Conditions as in Fig. 5.

nanoparticles after treatment. In contrast, our XPS and Raman analysis of the nZVI exposed to Cr(VI) suggest a structure, from outside to inside, of hydroxychromites → magnetite → Fe^0 and, thus, a decreasing Fe(III) and Cr(III) concentration gradient seems to be a more accurate model.

4. Conclusions

nZVI has been proven to be an efficient Cr(VI) removal agent that, combined with an alkaline precipitation step, should adjust chromium levels to current environmental regulations. Despite the remarkable Cr(VI) removal efficiency achieved by N25 particles, passivation of the nZVI surface showed to limit the removal capacity of the material. This effect is produced by an outer layer containing Fe(III)–Cr(III) mixed oxides/oxyhydroxides that prevents penetration of the pollutant and stops the electron transfer from inner Fe^0 to Cr(VI) in the aqueous phase. Raman and XPS analysis, combined with sputtering experiments, shed light over the composition of the external layer which, before treatment, is exclusively composed of mixed iron oxides (mainly magnetite); after the treatment, a structure of hydroxychromites → magnetite → Fe^0 is developed towards the core of the nZVI, together with a decreasing Fe(II) gradient.

Acknowledgements

This work was supported by Agencia Nacional de Promoción Científica y Tecnológica (ANPCyT, Argentina) PICT projects 512-2006 and 0463-2011. A special mention to Eng. Jan Slunský from NANO IRON, s.r.o. Contributions by Martha Ortiz to the TXRF measurements and Adriana Domínguez for SEM images are gratefully acknowledged.

Appendix A. Supplementary material

Experimental setup, characterization of N25 Fresh by XRD, Raman and SEM, XPS and additional fitting methodology are provided in the SD. Supplementary data associated with this article can be found, in the online version, at http://dx.doi.org/10.1016/j.cej.2014.01.093.

References

[1] B. Saha, C. Orvig, Biosorbents for hexavalent chromium elimination from industrial and municipal effluents, Coordin. Chem. Rev. 254 (2010) 2959–2972.
[2] WHO, Guidelines for drinking-water quality, fourth ed., World Health Organization, Geneva, 2011.
[3] A. Baral, R.D. Engelken, Chromium-based regulations and greening in metal finishing industries in the USA, Environ. Sci. Policy 5 (2002) 121–133.
[4] D.W. Blowes, C.J. Ptacek, J.L. Jambor, In-situ remediation of Cr(VI)-contaminated groundwater using permeable reactive walls: laboratory studies, Environ. Sci. Technol. 31 (1997) 3348–3357.
[5] R. Rangsivek, M.R. Jekel, Removal of dissolved metals by zero-valent iron (ZVI): kinetics, equilibria, processes and implications for stormwater runoff treatment, Water Res. 39 (2005) 4153–4163.
[6] M. Gheju, A. Iovi, Kinetics of hexavalent chromium reduction by scrap iron, J. Hazard. Mater. 135 (2006) 66–73.
[7] M.A. Hashim, S. Mukhopadhyay, J.N. Sahu, B. Sengupta, Remediation technologies for heavy metal contaminated groundwater, J. Environ. Manage. 92 (2011) 2355–2388.
[8] Y. Mamindy-Pajany, C. Hurel, F. Geret, M. Roméo, N. Marmier, Comparison of mineral-based amendments for ex-situ stabilization of trace elements (As, Cd, Cu, Mo, Ni, Zn) in marine dredged sediments: a pilot-scale experiment, J. Hazard. Mater. 252–253 (2013) 213–219.
[9] M. Gheju, I. Balcu, Removal of chromium from Cr(VI) polluted wastewaters by reduction with scrap iron and subsequent precipitation of resulted cations, J. Hazard. Mater. 196 (2011) 131–138.
[10] W.X. Zhang, Nanoscale iron particles for environmental remediation: an overview, J. Nanopart. Res. 5 (2003) 323–332.

[11] X.-Q. Li, W.-X. Zhang, Sequestration of metal cations with zerovalent iron nanoparticles a study with high resolution X-ray photoelectron spectroscopy (HR-XPS), J. Phys. Chem. C 111 (2007) 6939–6946.
[12] T. Pradeep, Anshup, Noble metal nanoparticles for water purification: a critical review, Thin Solid Films 517 (2009) 6441–6478.
[13] M.E. Morgada, I.K. Levy, V. Salomone, S.S. Farías, G. López, M.I. Litter, Arsenic (V) removal with nanoparticulate zerovalent iron: effect of UV light and humic acids, Catal. Today 143 (2009) 261–268.
[14] W. Yan, A.A. Herzing, C.J. Kiely, W.-X. Zhang, Nanoscale zero-valent iron (nZVI): aspects of the core–shell structure and reactions with inorganic species in water, J. Contam. Hydrol. 118 (2010) 96–104.
[15] R.A. Crane, T.B. Scott, Nanoscale zero-valent iron: future prospects for an emerging water treatment technology, J. Hazard. Mater. 211–212 (2012) 112–125.
[16] Y. Wu, J. Zhang, Y. Tong, X. Xu, Chromium (VI) reduction in aqueous solutions by Fe_3O_4-stabilized Fe^0 nanoparticles, J. Hazard. Mater. 172 (2009) 1640–1645.
[17] T.B. Scott, I.C. Popescu, R.A. Crane, C. Noubactep, Nano-scale metallic iron for the treatment of solutions containing multiple inorganic contaminants, J. Hazard. Mater. 186 (2011) 280–287.
[18] R.M. Powell, R.W. Puls, S.K. Hightower, D.A. Sabatini, Coupled iron corrosion and chromate reduction: mechanisms for subsurface remediation, Environ. Sci. Technol. 29 (1995) 1913–1922.
[19] R.W. Puls, D.W. Blowes, R.W. Gillham, Long-term performance monitoring for a permeable reactive barrier at the U.S. Coast Guard Support Center, Elizabeth City, North Carolina, J. Hazard. Mater. 68 (1999) 109–124.
[20] T. Lee, H. Lim, Y. Lee, J.W. Park, Use of waste iron metal for removal of Cr(VI) from water, Chemosphere 53 (2003) 479–485.
[21] J. Cao, W.X. Zhang, Stabilization of chromium ore processing residue (COPR) with nanoscale iron particles, J. Hazard. Mater. 132 (2006) 213–219.
[22] M. Gheju, Hexavalent chromium reduction with zero-valent iron (ZVI) in aquatic systems, Water Air Soil Pollut. 222 (2011) 103–148.
[23] B.A. Manning, J.R. Kiser, H. Kwon, S.R. Kanel, Spectroscopic investigation of Cr(III)- and Cr(VI)-treated nanoscale zerovalent iron, Environ. Sci. Technol. 41 (2006) 586–592.
[24] X.-Q. Li, J. Cao, W.-X. Zhang, Stoichiometry of Cr(VI) immobilization using nanoscale zerovalent iron (nZVI): a study with high-resolution X-ray photoelectron spectroscopy (HR-XPS), Ind. Eng. Chem. Res. 47 (2008) 2131–2139.
[25] Z. Ai, Y. Cheng, L. Zhang, J. Qiu, Efficient removal of Cr(VI) from aqueous solution with $Fe@Fe_2O_3$ core-shell nanowires, Environ. Sci. Technol. 42 (2008) 6955–6960.
[26] Q. Wang, N. Cissoko, M. Zhou, X. Xu, Effects and mechanism of humic acid on chromium(VI) removal by zero-valent iron (Fe^0) nanoparticles, Phys. Chem. Earth 36 (2011) 442–446.
[27] L. Alidokht, A.R. Khataee, A. Reyhanitabar, S. Oustan, Reductive removal of Cr(VI) by starch-stabilized Fe^0 nanoparticles in aqueous solution, Desalination 270 (2011) 105–110.
[28] J.-H. Kim, J.-H. Kim, V. Bokare, E.-J. Kim, Y.-Y. Chang, Y.-S. Chang, Enhanced removal of chromate from aqueous solution by sequential adsorption-reduction on mesoporous iron–iron oxide nanocomposites, J. Nanopart. Res. 14 (2012) 1–12.
[29] X. Lv, Y. Hu, J. Tang, T. Sheng, G. Jiang, X. Xu, Effects of co-existing ions and natural organic matter on removal of chromium (VI) from aqueous solution by nanoscale zero valent iron (nZVI)-Fe_3O_4 nanocomposites, Chem. Eng. J. 218 (2013) 55–64.
[30] C. Noubactep, A critical review on the process of contaminant removal in Fe^0-H_2O systems, Environ. Technol. 29 (2008) 909–920.
[31] B.A. Balko, P.G. Tratnyek, Photoeffects on the reduction of carbon tetrachloride by zero-valent iron, J. Phys. Chem. B 102 (1998) 1459–1465.
[32] M.M. Scherer, B.A. Balko, P.G. Tratnyek, The role of oxides in reduction reactions at the metal-water interface, in: ACS Symposium Series, 1998, pp. 301–322.
[33] C. Noubactep, A. Schöner, P. Woafo, Metallic iron filters for universal access to safe drinking water, Clean – Soil Air Water 37 (2009) 930–937.
[34] ASTM, Standards D 1687–92, 1999.
[35] E.B. Sandell, Colorimetric Determination of Trace Metals, Interscience Publishers Inc., New York, 1959. pp. 537–542.
[36] G. Custo, M.I. Litter, D. Rodríguez, C. Vázquez, Total reflection X-ray fluorescence trace mercury determination by trapping complexation: application in advanced oxidation technologies, Spectrochim. Acta Part B: Atom. Spectrosc. 61 (2006) 1119–1123.
[37] Z. Fang, X. Qiu, R. Huang, X. Qiu, M. Li, Removal of chromium in electroplating wastewater by nanoscale zero-valent metal with synergistic effect of reduction and immobilization, Desalination 280 (2011) 224–231.
[38] X. Lv, J. Xu, G. Jiang, J. Tang, X. Xu, Highly active nanoscale zero-valent iron (nZVI)–Fe_3O_4 nanocomposites for the removal of chromium(VI) from aqueous solutions, J. Colloid Interface Sci. 369 (2012) 460–469.
[39] F. dos Santos Coelho, J.D. Ardisson, F.C.C. Moura, R.M. Lago, E. Murad, J.D. Fabris, Potential application of highly reactive Fe(0)/Fe_3O_4 composites for the reduction of Cr(VI) environmental contaminants, Chemosphere 71 (2008) 90–96.
[40] A.F. White, M.L. Peterson, Reduction of aqueous transition metal species on the surfaces of Fe(II)-containing oxides, Geochimi. Cosmochim. Acta 60 (1996) 3799–3814.
[41] N. Melitas, O. Chuffe-Moscoso, J. Farrell, Kinetics of soluble chromium removal from contaminated water by zerovalent iron media: corrosion inhibition and passive oxide effects, Environ. Sci. Technol. 35 (2001) 3948–3953.
[42] R.M. Cornell, U. Schwertmann, Products of Iron Metal Corrosion, in: The Iron Oxides, Wiley-VCH Verlag GmbH & Co. KGaA, Darmstadt, 2004. pp. 491–508.
[43] J. Moulder, W. Stickle, P. Sobol, K. Bomben, Handbook of X-ray Photoelectron Spectroscopy, Eden Prairie, Minnesotta, 1992.